2D & 3D, CENTRED & OFFSET, CIRCULAR SYNTHETIC APERTURE SONAR POINT SPREAD FUNCTION

Yan Pailhas[a]

[a]NATO STO Centre for Maritime Research and Experimentation

Viale S. Bartolomeo 400, 19126 La Spezia, Italy
email: yan.pailhas@cmre.nato.int

Abstract: *It has become clear over the last decade that target multiview brings significant improvement in terms of recognition rate and false alarm reduction. New acquisition and re-acquisition patterns have since emerged for autonomous missions to bring additional views of targets of interest. One of them is circular SAS (Synthetic Aperture Sonar) acquisition also known as CSAS (Circular SAS) which has proven to be very efficient both in terms of acquisition time and image resolution. However the theory of CSAS has not been fully investigated. In this talk, we study the problem of the CSAS PSF (Point Spread Function) which is the fundamental brick of the coherent image formation. We will first derive the analytical formula for the 2D centred CSAS PSF before extending the formula to any point in the full field of view (offset point). We will then derive the PSF for any point for a 3D configuration. Although the PSF is not constant in the CSAS image, we will show that it is possible to derive a uniformisation scheme of the PSF for any point in the field of view. We will also demonstrate that the proposed uniformisation increases the SNR (Signal-to-Noise Ratio) of the resulting CSAS image.*

Keywords: *CSAS, Point Spread Function.*

1. INTRODUCTION

With the increased resolution provided by SAS (Synthetic Aperture Sonar) systems, ATR (Automatic Target Recognition) algorithms have become more reliable [1–3] by drastically improving the detection rate and diminishing the false alarm rate. However, the false alarm rate has to be lowered further to an acceptable level for a fully autonomous MCM system. Target multiview reacquisition may offer to ATR algorithms additional information to properly classify an object of interest. Among the reacquisition patterns, circular SAS acquisition also known as CSAS is of great interest [4–6] and has not been fully investigated yet. The problem of the PSF (Point Spread Function) of such system in particular remains. In [7] , the authors proposed an analytical expression of the CSAS PSF for the central point. This paper describes the derivation of PSF analytical formulas for offset points, i.e. all the points in the full filed of view. It also tackles the problem of the PSF in the 3D case and proposes a normalisation scheme that increase CSAS image SNR (Signal-to-Noise Ratio).

2. CSAS CONFIGURATION

2.1. Geometrical configuration

Let **S** be a SAS system performing a circle $\mathcal{C}$ centred in **O** and with a radius R. Let now **O'** be a point within the full view area (*i.e.* insonified by **S** during the full circular revolution). **OO'** can be written as αR where $\alpha \in [0, \alpha_{\max}]$ with $\alpha_{\max} \leq 1$. When **S** is in A, it has travelled a distance of θR from it original position, and *sees* the point **O'** at an angle θ'. θ and θ' are linked through equations (1) and (2).

$$\theta' = h(\theta) = \mathrm{sgn}(\theta)\cos^{-1}\left(\frac{\cos\theta - \alpha}{\sqrt{1+\alpha^2-2\alpha\cos\theta}}\right) \text{ and} \tag{1}$$

$$\theta = h^{-1}(\theta') = \mathrm{sgn}(\theta')\cos^{-1}\left(\alpha\sin^2\theta' + \cos\theta'\sqrt{1-\alpha^2\sin^2\theta'}\right). \tag{2}$$

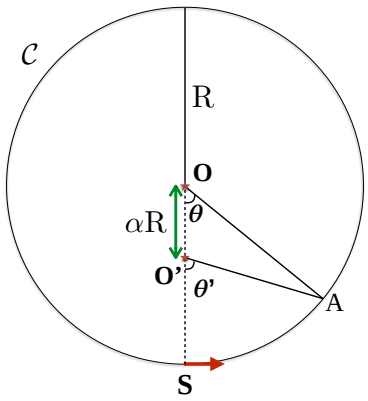

Fig. 1: (Color online) CSAS configuration and geometrical notations.

Figure 1 pictures the geometry and notations of the CSAS problem and the relationship between θ and θ'. Note that Eq. (2) and (1) are not linear. As a consequence, integrating along $\mathcal{C}$ is not uniform for **O'**. The PSF is then not uniform within the full view area.

2.2. CSAS parameters and centre point PSF

The CSAS centre point PSF has been analytically derived in [7]. We recall here some of the results needed for the calculation of the offset PSF. Let $p(t)$ be the transmitting pulse. Assuming a Gaussian weighted LFM (Linear Frequency Modulated) signal, $p(t)$ writes as

$$p(t) = \exp\left(-\frac{t^2}{2\sigma^2}\right)\exp\left[2i\pi\left(f_0+\frac{\Delta f}{2T}t\right)t\right]. \tag{3}$$

where T is the pulse duration, f_0 the central frequency and Δf the bandwidth. The matched filter response $p_{\mathrm{MF}}(t)$ of (3) is given by

$$p_{\mathrm{MF}}(t) = B(t)\, e^{2i\pi f_0 t}, \text{ where } B(t) = \sigma\sqrt{\pi}\exp\left[-\left(\frac{1}{4\sigma^2}+\pi^2\frac{\Delta f^2}{T^2}\sigma^2\right)t^2\right]. \tag{4}$$

We can see from (4) that the matched filter response $p_{\mathrm{MF}}(t)$ is only a low frequency envelope, $B(t)$, modulated by the central frequency f_0. The frequency content of $p_{\mathrm{MF}}(t)$ then comes from the frequency leakage caused by $B(t)$. The derivation of the point spread function I at the centre point $\mathbf{O}$ is obtained by integrating (4) along $\mathcal{C}$. Thanks to the problem symmetry, $I = I(r)$ is only function of r (distance to the centre $\mathbf{O}$), and can be analytically calculated:

$$I(r) = 2\pi B\left(\frac{2r}{c}\right)J_0(2kr), \tag{5}$$

where $k = 2\pi f_0/c$ is representing the wave number and $J_0(.)$ the Bessel function of the first kind of order 0. The 2D Fourier transform $\hat{I}(\rho)$ of (5) can also be calculated analytically in the special polar coordinates:

$$\hat{I}(\rho) = 4\pi^{5/2}a_0^2\sigma\exp\left[-2a_0^2(k^2+\pi^2\rho^2)\right]I_0(4\pi k a_0^2\rho) \tag{6}$$

where $a_0 = \frac{1}{\sqrt{2}}\frac{c\sigma T}{\sqrt{T^2+4\pi^2\Delta f^2\sigma^4}}$ and $I_0(.)$ represents the modified Bessel function of the first kind at the order 0. Eq. (6) can be well approximated:

$$\hat{I}(\rho) \approx \pi^2\sqrt{2}\frac{a_0\sigma}{k}\exp\left[-2a_0^2(k-\pi\rho)^2\right]. \tag{7}$$

We can see that, in the Fourier domain, the CSAS PSF is a Gaussian ring with a diameter of $2f_0/c$ and a variance of $1/\pi^2a_0^2$. Note that $\hat{I}(\rho) \in \mathbb{R}$

3. THE OFFSET POINT PSF PROBLEM

In coherent imaging, the PSF plays a central role in the understanding of the resolution problem. It is in essence the founding pillar of the image formation. The direct integration of (4) along $\mathcal{C}$ for any offset point to compute the generalised PSF within the full view area is not analytically trackable. This section extends the result given by (7) to offset points using a plane wave assumption. The justification of the plane wave assumption comes from the ratio between the expected radius of the PSF (in the order of few λ, where λ represents the wavelength) and the distance between the imaged point and the sensor (in the order of tens of metres). For example, assumming a PSF of 5λ radius and a ranging distance of 40m, the maximum error due to the plane wave assumption is less than $5.10^{-3}\lambda$, which represents more that one order of magnitude lower compared to the classic $\lambda/8$ needed for coherent processing.

3.1. Offset CSAS PSF

We saw in section 2.1 that the PSF is not uniform across the full imaging area. Let (x_0, y_0) the Cartesian coordinates of $\mathbf{O}'$. Under plane wave assumption, the CSAS PSF at $\mathbf{O}'$ can be written as

$$I(x,y) = \int_C B\left(2\frac{(x-x_0)\cos\theta' - (y-y_0)\sin\theta'}{c}\right)\exp\left[ik((x-x_0)\cos\theta' - (y-y_0)\sin\theta')\right]d\theta. \tag{8}$$

Let

$$\xi(x,y,\theta') = B\left(2\frac{(x-x_0)\cos\theta' - (y-y_0)\sin\theta'}{c}\right)\exp\left[ik((x-x_0)\cos\theta' - (y-y_0)\sin\theta')\right] \tag{9}$$

be the integrand of (8), and $(\alpha R, \theta_0)$ be the polar coordinates of $\mathbf{O}'$. The Fourier transform of (9) then writes as::

$$\hat{\xi}(\rho,\phi,\theta') = \pi\sqrt{2}a_0\sigma\exp\left[-2a_0^2(\pi\rho - k)^2\right]\exp(i\Phi)\delta(\phi+\theta'+\pi/2), \tag{10}$$

where $\Phi = 2\pi\rho\alpha R\cos(\theta_0 - \phi)$ is the offset phase shift. Note that the expression in (10) is perfectly intuitive: the Dirac function $\delta(.)$ came from the $\exp(.)$ expression in (9) and the Gaussian window from $B(.)$. Eq. (10) is in essence a slide in the k-space where only one angle contributes. It is important to note that $\{\hat{\psi}\}_{\theta'}$ is in essence a wavelet basis which reconstructs exactly the PSF given by (7). Variable manipulation in (8) leads to:

$$\mathrm{FFT}[I] = \hat{I}(\rho,\phi) = \int_{\theta=-\pi}^{+\pi}\hat{\xi}(\rho,\phi,\theta')d\theta = \int_{\theta'=-\pi}^{+\pi}\hat{\xi}(\rho,\phi,\theta')g(\theta')d\theta', \tag{11}$$

where

$$g(\theta') = \frac{\mathrm{d}h^{-1}(\theta')}{\mathrm{d}\theta'} = \frac{\sin\theta'\sqrt{1-\alpha^2\sin^2\theta'} + \frac{\alpha^2\cos^2\theta'\sin^2\theta'}{\sqrt{1-\alpha^2\sin^2\theta'}} - 2\alpha\cos\theta'\sin\theta'}{\sqrt{1-\left(\cos\theta'\sqrt{1-\alpha^2\sin^2\theta'} + \alpha\sin^2\theta'\right)^2}} \tag{12}$$

The first order of the MacLaurin series of (12) reduces to:

$$g(\theta') = 1 - \alpha\cos\theta' + O(\alpha^2). \tag{13}$$

Using finally (10) with (11) gives the general CSAS PSF:

$$\hat{I}(\rho,\phi) = \sqrt{2}\pi\sigma a_0\exp\left[-2a_0^2(\pi\rho - k)^2\right]\exp(i\Phi)\ g(\phi+\theta_0+\pi/2). \tag{14}$$

The two PSF expressions for an offset point given by (14) and for the central point only differ by the angular weighting factor $g(\phi+\theta_0+\pi/2)$. Figure 2(a) plots a 3D representation of the spectral CSAS PSF for an offset point with the parameters $\alpha = \frac{1}{\sqrt{2}}$ and $\theta_0 = 45°$ computed directly. As expected, the PSF in the Fourier domain is no longer symmetric and exhibits a strong angular dependency.

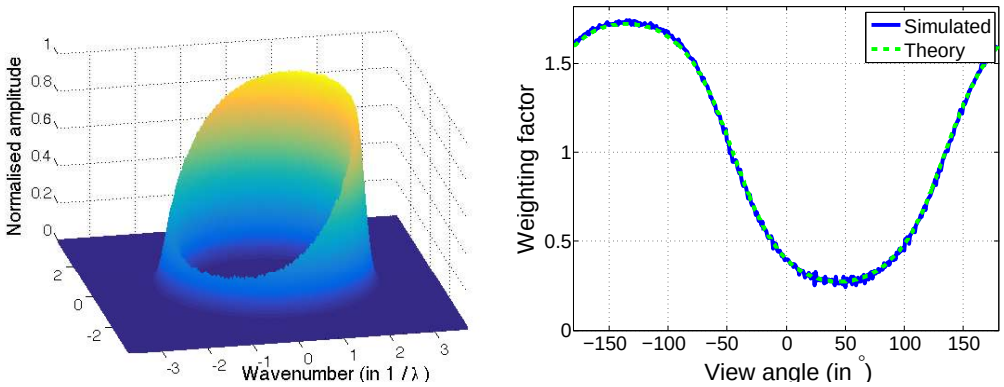

(a) (b)

Fig. 2: (a) 3D plot of the normalised Fourier transform of an offset point. (b) Angular weighting factor for simulated data and the theoretical expression (14)*.*

3.2. PSF normalisation

Figure 2(b) compares the angular weighting coefficient between the simulated data plotted in figure 2(a) and the theoretical value $g(.)$ from Eq. (12). Set apart the noise coming from the numerical simulation, the simulated and theoretical curves match extremely well. Now that the CSAS PSF for any point of the full view area has been fully characterised, and in particular the angular weighting dependency, it is possible to make the CSAS PSF uniform everywhere within the full view area by simply correcting the angular weighting factor. The discrete implementation of the angular compensation can be written as:

$$I(\mathbf{O}') = \sum_{n=1}^{N} \frac{1}{g(\theta_n - \theta_0)} s_{\mathrm{MF}}^{\theta_n}(t), \tag{15}$$

where N represents the total number of views obtained along the circular acquisition. Figure 3 plots the image spectra of the same offset point as figure 2(a) corrected using the proposed scheme (15). Note that the PSF is now symmetrical similarly to the central point PSF.

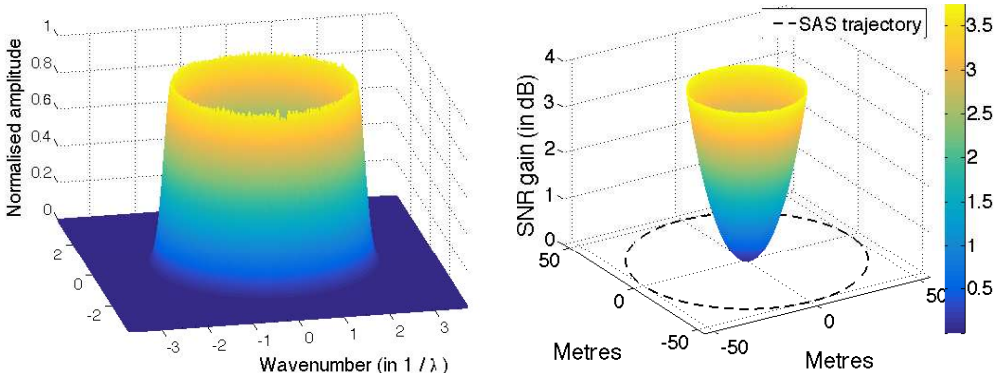

(a) (b)

Fig. 3: (a) 3D plot of the normalised Fourier transform of an offset point corrected using (15)*. (b) SNR increase for the full field of view after PSF normalisation.*

The normalisation proposed by (15) also offers an unexpected advantage: by weighting more heavily the acquisitions where the SAS system is closer to the offset point, the uniformisation (15) increases the SNR (Signal-to-Noise Ratio). The SNR provided by the CSAS processing without normalisation can be written as:

$$\mathrm{SNR} \propto \int_{\theta=0}^{2\pi} \frac{\mathrm{d}\theta}{\mathbf{O}'\mathbf{A}^2(\theta)} = \frac{2\pi}{1-\alpha^2}. \tag{16}$$

By applying (15), the SNR can be calculated by performing a Taylor series decomposition and using the simplified expression (13) for the correction factor $g(.)$ and then becomes:

$$\mathrm{SNR}_{\mathrm{corr}} \propto \int_{\theta=0}^{2\pi} \frac{\mathrm{d}\theta}{g(\theta-\theta_0)\mathbf{O}'\mathbf{A}^2(\theta)} \approx \frac{9\pi}{4(1-\alpha^2)^{9/4}} - \frac{\pi}{4}. \tag{17}$$

The increase in SNR (expressed in dB) due to the proposed uniformisation is then approximately

$$\mathrm{SNR}_{\mathrm{inc}} \approx -30\log_{10}(1-\alpha^2). \tag{18}$$

Figure 3(b) shows the SNR increase depending on the location within the full field of view. It is interesting to note that the SNR gain can be significant (up to few dBs as shown in figure 3(b)). It is also worth mentioning that higher SNR is observed the further away from the central point.

4. THE 3D CENTRED & OFFSET POINT PSF PROBLEM

We first consider the 3D centred PSF problem. Let ψ be the grazing angle of the pulse. ψ is constant for the full revolution and can be computed with

$$\psi = \tan^{-1}\left(\frac{h}{R}\right) \tag{19}$$

where h is the high of the SAS system. We can derive $I(r)$ from Eq. (5) by writing:

$$I(r) = 2\pi B\left(\frac{2r}{c}\cos\psi\right) J_0(2kr\cos\psi). \tag{20}$$

For offset point, and similarly to the derivations of section 3, the PSF is not constant and not directly trackable. The expression of the 3D offset PSF can be found in the special domain using the plane wave assumption:

$$\hat{I}(\rho) = \frac{2\pi^{3/2}}{\cos^{3/2}\psi}\frac{\sigma a_0}{\sqrt{2k\rho}}\exp\left[-2a_0^2\left(\frac{\pi\rho}{\cos\psi}-k\right)^2\right] \tag{21}$$

where this time ψ is function of θ and reads as

$$\psi(\theta) = \tan^{-1}\left(\frac{h}{R(1-2\alpha\cos\theta+\alpha^2)^{1/2}}\right). \tag{22}$$

5. CONCLUSIONS

The analytical derivation of the PSF of 2D and 3D case, for central and offset points has been proposed. We showed that full coherent CSAS can be normalised such as the PSF becomes uniform for the full field of view.

ACKNOWLEDGEMENT

This work was performed under the Project SAC000905–High Resolution Low Frequency Synthetic Aperture Sonar (HRLFSAS) of the STO-CMRE Programme of Work, was funded by the NATO Allied Command Transformation.

REFERENCES

[1] Y. Pailhas, Y. Petillot, and C. Capus. High-resolution sonars: What resolution do we need for target recognition? *EURASIP J. Adv. Signal Process.*, 2010(1):205095, 2010.

[2] J. Sawas, Y. Petillot, and Y. Pailhas. Cascade of boosted classifiers for rapid detection of underwater objects. In *Proceedings of the European Conference on Underwater Acoustics*, pages 1507–1516. Institute of Acoustics, St Alban, UK, 2010.

[3] V. Myers and J. Fawcett. A template matching procedure for automatic target recognition in synthetic aperture sonar imagery. *IEEE Signal Process. Lett.*, 17(7):683–686, 2010.

[4] B. G. Ferguson and R. J. Wyber. Application of acoustic reflection tomography to sonar imaging. *J. Acoust. Soc. Am.*, 117(5):2915–2928, 2005.

[5] T. M. Marston, J. L. Kennedy, and P. L. Marston. Autofocusing circular synthetic aperture sonar imagery using phase corrections modeled as generalized cones. *J. Acoust. Soc. Am.*, 136(2):614–622, 2014.

[6] D. S. Plotnick, P. L. Marston, and T. M. Marston. Fast nearfield to farfield conversion algorithm for circular synthetic aperture sonar. *J. Acoust. Soc. Am.*, 136(2):EL61–EL66, 2014.

[7] Y. Pailhas, Y. Petillot, and B. Mulgrew. Increasing circular synthetic aperture sonar resolution via adapted wave atoms deconvolution. *J. Acoust. Soc. Am.*, 141(4):2623–2632, 2017.